Original

Nueske, R.; Jurgilaitis, A.; Enquist, H.; Farahani, S.D.; Gaudin, J.; Guerin, L.; Harb, M.; Korff Schmising, C.v.; Stoermer, M.; Wulff, M.; Larsson, J.:

Picosecond time-resolved x-ray refectivity of a laser-heated amorphous carbon film

In: Applied Physics Letters (2011) AIP

DOI: 10.1063/1.3562967

Combined x-ray photoelectron spectroscopy and scanning electron microscopy studies of the $LiBH_4-MgH_2$ reactive hydride composite with and without a Ti-based additive

E. Deprez,[1] M. A. Muñoz-Márquez,[1,a)] M. C. Jimenez de Haro,[1] F. J. Palomares,[2] F. Soria,[2] M. Dornheim,[3] R. Bormann,[3] and A. Fernández[1,b)]
[1]*Instituto de Ciencia de Materiales de Sevilla (CSIC-Univ.Sevilla), Avda. Américo Vespucio 49, 41092 Seville, Spain*
[2]*Instituto de Ciencia de Materiales de Madrid, CSIC, Cantoblanco, 28049 Madrid, Spain*
[3]*Institute of Materials Research, Helmholtz-Zentrum Geesthacht GmbH, Max-Planck-Str. 1, D-21502 Geesthacht, Germany*

(Received 9 September 2010; accepted 9 November 2010; published online 10 January 2011)

A detailed electronic and microstructural characterization is reported for the $LiBH_4-MgH_2$ reactive hydride composite system with and without titanium isopropoxide as additive. Surface characterization by x-ray photoelectron spectroscopy combined to a morphological study by scanning electron microscopy as well as elemental map composition analysis by energy dispersive x-ray emission are presented in this paper for the first time for all sorption steps. Although sorption reactions are not complete at the surface due to the unavoidable superficial oxidation, it has been shown that the presence of the additive is favoring the heterogeneous nucleation of the MgB_2 phase. Ti-based phases appear in all the samples for the three sorption steps well dispersed and uniformly distributed in the material. Li-based phases are highly dispersed at the surface while the Mg-based ones appear, either partially covered by the Li-based phases, or forming bigger grains. Ball milling is promoting mixing of phases and a good dispersion of the additive what favors grain refinement and heterogeneous reactions at the interfaces. © *2011 American Institute of Physics*.
[doi:10.1063/1.3525803]

I. INTRODUCTION

Hydrogen as energy carrier combined to fuel cells represents an efficient and clean solution for meeting the power demands in portable applications.[1] The challenge is to make hydrogen safe and reliable for automotive applications. The U.S. Department of Energy (DOE) imposed high gravimetric and volumetric storage densities for transportation application (9.0 wt % and 91 kg m^{-3} for 2015).[2] Up to now, several classes of candidates as hydrogen storage materials have been investigated including metal hydrides,[1,3–6] chemical hydrides,[7,8] organometallic complexes,[9] etc. Among them the lithium borohydride $LiBH_4$ appears to be a potential candidate due to its high hydrogen storage capacities (18.3 wt %, 121 kg m^{-3}) which theoretically could fulfil the DOE requirements. However, $LiBH_4$ is rather stable and the dehydrogenation reaction proceeds only at elevated temperatures.[7,10–12] Recently it has been reported that by combination with magnesium hydride MgH_2, MgB_2 is formed during the desorption reaction; the overall reaction enthalpy is, therefore, lowered and allows for lower reaction temperatures keeping the high hydrogen storage capacity.[13,14] The reaction, which has been shown to be reversible, releases about 10.5 wt % of hydrogen according to the desorption reaction, as follows:

$$2LiBH_4 + MgH_2 \leftrightarrow 2LiH + MgB_2 + 4H_2. \quad (1)$$

The system is known as a typical reactive hydride composite (RHC) (Refs. 13 and 14) and shows a two step kinetics for desorption. First MgH_2 desorbs and forms Mg. After an incubation period the $LiBH_4$ decomposes leading simultaneously to the formation of LiH and MgB_2 with additional hydrogen release.[15,16] It has been demonstrated that MgB_2 formation is the key for the reversibility.[14,17] To reach the DOE requirements, the dehydrogenation/hydrogenation of the system needs to be improved to reduce the incubation period as well as the overall reaction kinetics. Several additives such as transition metal oxides or chlorides have been proved to significantly reduce the incubation period.[14] The organometallic compound titanium isopropoxide (Ti-iso) was found to be one of the most efficient additives for this system.[15,16] Additionally the initial activation and mixing of materials and additives by high energy ball milling is also contributing strongly to kinetic improvement.[15,16]

The characterization of the additives in the initial and cycled composites was a first step toward understanding the function of additives and the mechanism of H_2 sorption reactions.[18–21] It has been demonstrated that additives evolve during milling and/or first desorption to form metal boride nanoparticles. These particles act as nucleation sites for the heterogeneous nucleation of the MgB_2 phase what makes the kinetic faster and reduce strongly the incubation period for the second desorption step. In the case of Ti-based additives we have demonstrated that the additive reduces from Ti(IV) oxide in the as milled sample to form the active TiB_2 species

a)Present address: Centro de Física de Materials (EHU-CSIC), Paseo Manuel de Lardizabal 5, 20018 San Sebastián, Spain.
b)Electronic mail: asuncion@icmse.csic.es.

during the first desorption reaction. At the same time the additive species migrate to the bulk where they favor heterogeneous reactions at the interface of reactants.[20] Additionally a recent exhaustive microstructural characterization for the $2LiBH_4-MgH_2$ RHC system with and without the Ti-iso additive[22] has shown that microstructural effects, related to the high dispersion of titanium-based additives, result in a distinct grain refinement of MgB_2 and an increase in the number of reaction sites, causing acceleration of desorption and absorption reactions.

In this work it is shown a detailed study of the surface composition and the oxidation states in the $LiBH_4-MgH_2$ composite by x-ray photoelectron spectroscopy combined to a morphological study by scanning electron microscopy (SEM) as well as elemental map composition analysis by energy dispersive x-ray emission (EDX). Samples have been characterized after ball milling, desorption and one cycle and the influence of the Ti-iso additive has been investigated by comparison of the system with and without additive. No previous results have been presented by this combination of techniques on the $LiBH_4-MgH_2$ RHC system. New data are reported regarding microstructural characterization, grain size, surface composition, and elemental distribution in the microscale. Data are compared to previous results by X-ray absorption spectroscopy (XAS), x-ray diffraction (XRD), transmission electron microscopy (TEM), selected-area electron diffraction (SAED), and electron energy loss spectroscopy (EELS) in Refs. 18–22. The new results in this paper will contribute to the understanding of the reaction mechanism and the influence of the additives on the kinetics.

II. EXPERIMENTAL

A. Sample preparation

Samples were prepared by high energy ball milling in a Spex 8000 mixer mill using a ball (steel) to powder ratio of 10:1. The initial microcrystalline powders, Lithium borohydride $LiBH_4$ (95% purity), Magnesium hydride MgH_2 (98% purity, the rest being Mg) and titanium isopropoxide Ti-iso (99.995% purity) were purchased from Alfa Aesar. Microcrystalline powders used as reference samples, lithium hydride LiH (99.4% purity) and Magnesium boride MgB_2 were produced by Alfa Asear.

MgH_2 was previously milled for 5 h before being mixed with $LiBH_4$ and 5 or 10 mol % of Ti-iso for a further 5 h milling. A set of samples without additive was also prepared to be used for comparison. For the preparation of samples at the different sorption stages, hydrogen cycling was performed in a thermovolumetric Sieverts apparatus designed by Hydro Quebec/HERA Hydrogen Storage System. Desorption and absorption reactions were performed, respectively, at 400 °C and 350 °C under 5 and 50 bar hydrogen.[15]

Preparation and handling were performed under continuously purified argon or nitrogen atmosphere in glove boxes.

B. Sample characterization

TEM analysis was performed in a Philips CM200 microscope operating at 200 kV and equipped with an EDX detector. Samples were diluted into dried toluene inside the glove box, dropped onto a copper grid and introduced into the microscope. A vacuum gate valve allowed the sample to be isolated in a prechamber for complete evaporation of toluene prior to transfer for analysis.

SEM analysis was performed in a high resolution field emission gun microscope HITACHI S 4800 operating at 2 kV. For EDX spectroscopy a voltage of 5 kV has been applied. The EDX detector also allows the registration of individual elemental mapping. Samples were diluted into dried hexane inside the glove box, dropped onto a copper grid and introduced into the microscope. A vacuum gate valve allowed the sample to be isolated in a prechamber for complete evaporation of hexane before transfer for analysis. For elemental mapping samples containing 10 mol % Ti-iso have been used to ensure a good signal for Ti elemental maps. Distribution of B, O, Ti, and Mg elements are presented.

XRD measurements were performed with a powder diffractometer Siemens D5000-D with a goniometer for transmission geometry and carried out with Cu-Kα radiation. The samples were sealed in a glass capillary inside the glovebox. Data acquisition was performed for 2θ angle range of 15°–90°.

XPS spectra were recorded with a SPECS Phoibos150 electron spectrometer and a Delay Line Detector in the nine segmented mode, using Al Kα radiation (1486.6 eV) in an ultrahigh vacuum chamber at a base pressure of 6×10^{-10} mbar. Li 1*s*, Mg 2*p*, Mg *KLL*, *B* 1*s*, and Ti 2*p* core level XPS spectra were acquired with 20 eV pass energy and 0.5 eV energy step at normal emission take-off angle. The binding energy reference was taken as the main component of the C 1*s* peak at 284.6 eV for a mixture of adventitious carbon.

The Auger parameter α has been calculated for the Mg species using the following equation:

$$\alpha(\mathrm{Mg}) = \mathrm{BE}(\mathrm{Mg}\ 2p) + \mathrm{KE}(\mathrm{Mg}\ KLL), \quad (2)$$

where BE(Mg 2*p*) is the binding energy of the Mg 2*p* peak and KE(Mg *KLL*) is the kinetic energy of the Mg auger peak.

Powder samples were deposited onto adhesive Cu substrates inside the glove box and transported in N_2 atmosphere to the XPS spectrometer. A portable glove box was coupled to the XPS load-lock chamber to avoid air exposure of the samples.

III. RESULTS

A. Description of investigated samples

The RHC $2LiBH_4+MgH_2$ desorption was found to occur according to reaction (1) (see introduction section). In this work RHC samples will be characterized in three steps: (i) as prepared by high energy ball milling of $2LiBH_4+MgH_2$ (with and without additive), (ii) after desorption, and (iii) after one hydrogen cycle (hydrogen absorption after first desorption). Samples without and with 5 or 10 mol % Ti-iso will be compared and are summarized in Table I with their corresponding labels.

X-ray diffraction has been carried out to identify the different crystalline phases present and to check completion

TABLE I. Summary of investigated samples and labels.

Label	Samples	Condition
M_1	$2LiBH_4+MgH_2$ after ball milling	Untreated surface
M_2	$2LiBH_4+MgH_2$ after desorption	Untreated surface
M_3	$2LiBH_4+MgH_2$ after 1 cycle	Untreated surface
M_{1-10Ti}	$2LiBH_4+MgH_2$+10 mol% Ti-iso after ball milling	Untreated surface
M_{2-10Ti}	$2LiBH_4+MgH_2$+10 mol% Ti-iso after desorption	Untreated surface
M_{3-10Ti}	$2LiBH_4+MgH_2$+10 mol% Ti-iso after 1 cycle	Untreated surface
M_{1-5Ti}	$2LiBH_4+MgH_2$+5 mol% Ti-iso after ball milling	Untreated surface
M_{2-5Ti}	$2LiBH_4+MgH_2$+5 mol% Ti-iso after desorption	Untreated surface
M_{3-5Ti}	$2LiBH_4+MgH_2$+5 mol% Ti-iso after 1 cycle	Untreated surface
$^{Ar+}M_{1-5Ti}$	$2LiBH_4+MgH_2$+5 mol% Ti-iso after ball milling	Alter 1 h Ar^+ sputtering
$^{Ar+}M_{2-5Ti}$	$2LiBH_4+MgH_2$+5 mol% Ti-iso after desorption	Alter 1 h Ar^+ sputtering
$^{Ar+}M_{3-5Ti}$	$2LiBH_4+MgH_2$+5 mol% Ti-iso after 1 cycle	Alter 1 h Ar^+ sputtering

for the different sorption stages. Figure 1 shows XRD patterns of $2LiBH_4+MgH_2$ and $2LiBH_4+MgH_2$+5 mol% Ti-iso after ball milling (a), desorption (b), and reabsorption (c) with indication of the expected peak positions for reference materials indexed in the upper part. After ball milling, main peaks corresponding to β-MgH_2 and $LiBH_4$ phases are clearly identified in both samples. The possible formation of MgO phases cannot be detected in the as milled materials due to the amorphous character of oxide passivation layers[23] before the heating sorption steps. The diffractograms intensity in presence of Ti-iso is found to be smaller due to the absorption of Ti atoms and the transmission geometry of the diffraction measurements. After desorption [Fig. 1(b)] LiH and MgB_2 phases are observed; the presence of MgO is confirmed especially in the sample containing the Ti-iso additive which is the main source of oxygen in these samples. After one cycle [Fig. 1(c)] the major peaks are indexed as β-MgH_2 and $LiBH_4$ phases what confirms the reversibility of the reaction described above. MgO presence is found even more visible for the sample with Ti-iso additive after one cycle due to the crystallization of amorphous oxide phases upon heating. A detailed analysis of the XRD data has been presented in Ref. 22.

In the three sorption states, no crystalline Ti phases were identified by XRD which shows the advantage of using techniques as x-ray photoelectron spectroscopy to study the role of the additive and the surface composition.

B. X-Ray Photoelectron analysis

XPS analysis was carried out to investigate the chemical composition of the surface of the investigated samples and to

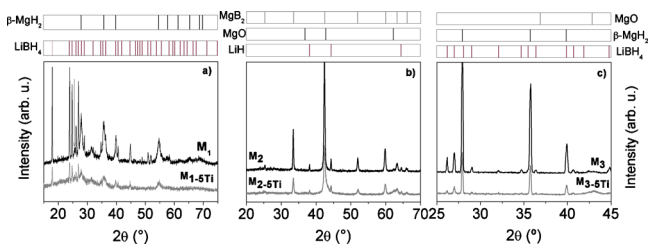

FIG. 1. (Color online) XRD patterns of $2LiBH_4+MgH_2$ and $2LiBH_4+MgH_2$+5 mol % Ti-iso after ball milling (a), after desorption (b), and one cycle (c). Peaks of references are indexed above: tetragonal MgH_2 (β-MgH_2), orthorhombic $LiBH_4$, cubic MgO, hexagonal MgB_2, and cubic LiH.

study the influence of the additive by comparing samples with and without Ti-iso. The intensity of XPS signals are characterized by an exponential decay from surface to bulk given by the mean free path of photoelectrons of a particular kinetic energy in each particular material.[24] In our measurements we estimate an analysis depth by XPS of around 50 Å from the surface. Samples without additive (M_1, M_2, and M_3) have been analyzed and compared to samples with 5 mol % Ti-iso at the same sorption stages (M_{1-5Ti}, M_{2-5Ti}, and M_{3-5Ti}) according to labeling shown in Table I. Additionally a study of the subsurface layers of the samples with additive has been carried out by doing the XPS analysis after 1 h Ar^+ sputtering (samples $^{Ar+}M_{1-5Ti}$, $^{Ar+}M_{2-5Ti}$, and $^{Ar+}M_{3-5Ti}$ in Table I). The estimated value of removed material during sputtering is in the order of magnitude of few hundreds of nanometer.

First reference samples (MgB_2, MgH_2, $LiBH_4$, LiH, TiO_2, and TiB_2) were analyzed to be compared to the RHC materials. The Li 1*s*, Mg 2*p*, B 1*s*, and Ti 2*p* photoelectron peaks have been registered. Figure 2 shows the Li 1*s* photoemission peak in LiH and $LiBH_4$, the Mg 2*p* photoemission peak in MgH_2 and MgB_2, the B 1*s* photoemission peak in $LiBH_4$ and MgB_2 and the Ti 2*p* photoemission peak in TiO_2 and TiB_2. The binding energy positions of the deconvoluted peaks and their corresponding chemical species identified for Li, B, and Mg are summarized in Table II. At this point it is important to consider that due to surface reactivity, unavoidable oxidized species will be detected by XPS in all analyzed samples.

The Li 1*s* photoemission peaks in LiH and $LiBH_4$ references show a single component identified as the contribution of the hydride and the associated oxide. It has been shown that binding energies of a hydride and its associated oxide overlap[23] and it is difficult to distinguish both contributions without using x-ray synchrotron radiation sources.[25] LiH/Li_2O species show a Li 1*s* peak at 55.0 eV in LiH (Refs. 26 and 27) whereas in $LiBH_4$ the Li 1*s* peak at 56.2 eV reported here is identified as $LiBH_4/LiB_xO_y$.

In MgH_2 only one peak at 49.8 eV for Mg 2*p* is identified as the hydride and oxide components have overlapping of this photoelectron peak.[23] The Mg Auger parameter

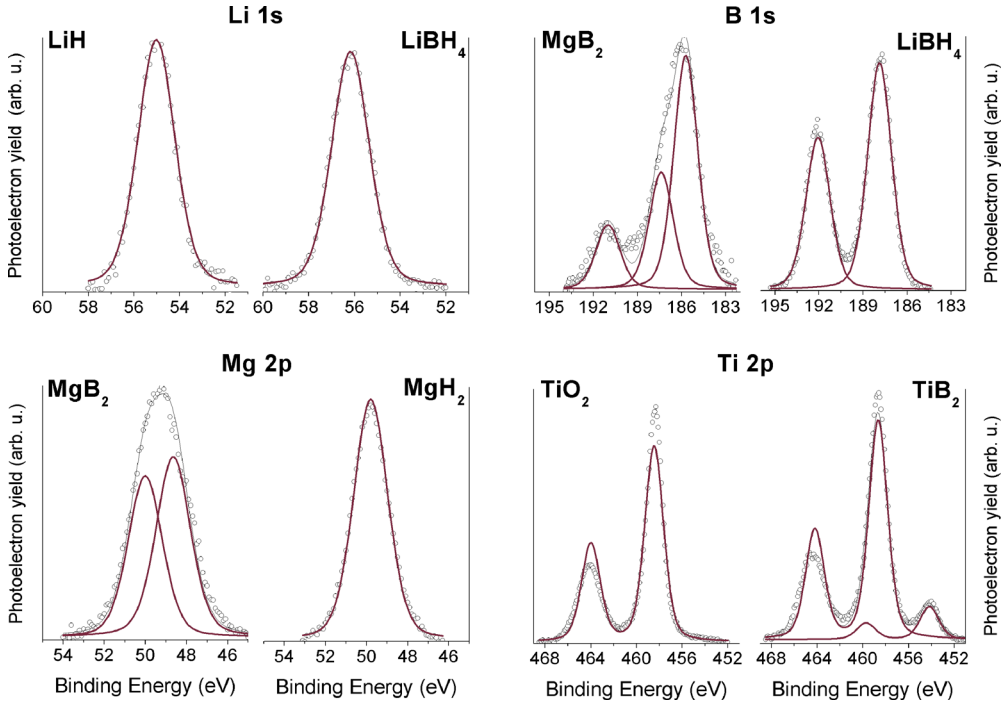

FIG. 2. (Color online) Li 1*s*, B 1*s*, Mg 2*p*, and Ti 2*p* photoemission spectra for references samples: LiH, $LiBH_4$, MgH_2, MgB_2, TiO_2, and TiB_2.

calculated for the MgH_2/MgO species in the reference materials is, according to data in Table II, 1231.4 eV which is close to the value obtained by Vasquez *et al.*[28] found to be equal to 1230.9 eV.

In magnesium diboride, MgB_2, the Mg 2*p* peak can best be fitted by assuming two different chemical states at 48.6 and 49.9 eV. The contribution at lower binding energy is attributed to MgB_2 whereas the one at higher energy corresponds to magnesium oxide MgO (formed by surface oxidation of the reference material) and was found close to the one identified in MgH_2 and in agreement to the literature.[28,29] In Table II are also indicated the two Mg KLL peaks of MgB_2 and MgO species. The Auger parameter for the MgO is found equal to 1231.2 eV in agreement with the value for the MgH_2/MgO reference material and the literature data.[28] The Auger parameter corresponding to MgB_2 is evaluated to be 1234.9 eV in our measurements in agreement with the 1234.35 and 1234.6 eV values found respectively by Vasquez *et al.* and Serquis *et al.*[28,30]

The B 1*s* peak in $LiBH_4$ shows two different chemical states: the hydride phase and the associated oxide. The hydride phase $LiBH_4$ appears at 187.8 eV whereas the oxide phase at 192.0 eV corresponds to B_2O_3 which are both in agreement with the literature values.[31] In MgB_2, three different contributions are clearly distinguished: magnesium diboride MgB_2 and two oxides. MgB_2 appears in the B 1*s* at 185.8 eV and its oxides at 187.4 and 191.1 eV which are identified to the oxides B_xO_y $(x/y=3)$ and B_xO_y $(1.5<x/y<3)$ according to the literature.[32]

The TiO_2 reference shows the Ti 2*p* doublet with a Ti 2*p 3/2* at 458.5 eV characteristic of TiO_2 photoemission peaks.[31] In TiB_2 two different chemical states of Ti are iden-

TABLE II. Summary of XPS core level binding energies (Li 1s, B 1s, Mg 2p) and Auger electron kinetic energy (Mg KLL) for the reference samples MgB2, MgH2, LiBh4 and LiH with indication of the corresponding chemical species.

	Li 1s		B 1s		Mg 2p		Mg KLL	
	Position B.E. (eV)	Chemical Specie	Position B.E. (eV)	Chemical Specie	Position B.E. (eV)	Chemical Specie	Position B.E. (eV)	Chemical Specie
			185.8	MgB_2	48.6	MgB_2	1186.3	MgB_2
					49.9	MgO	1181.3	MgO
MgB_2			187.4	B_xO_y $(x/y=3)$				
			191.1	B_xO_y $(1.5<x/y<3)$				
MgB_2					49.8	MgH_2/MgO	1181.6	MgH_2/MgO
$LiBH_4$	56.2	$LiBH_4/LiB_xO_y$	187.8	$LiBH_4$				
			192.0	B_2O_3				
LiH	55.0	LiH/Li_2O						

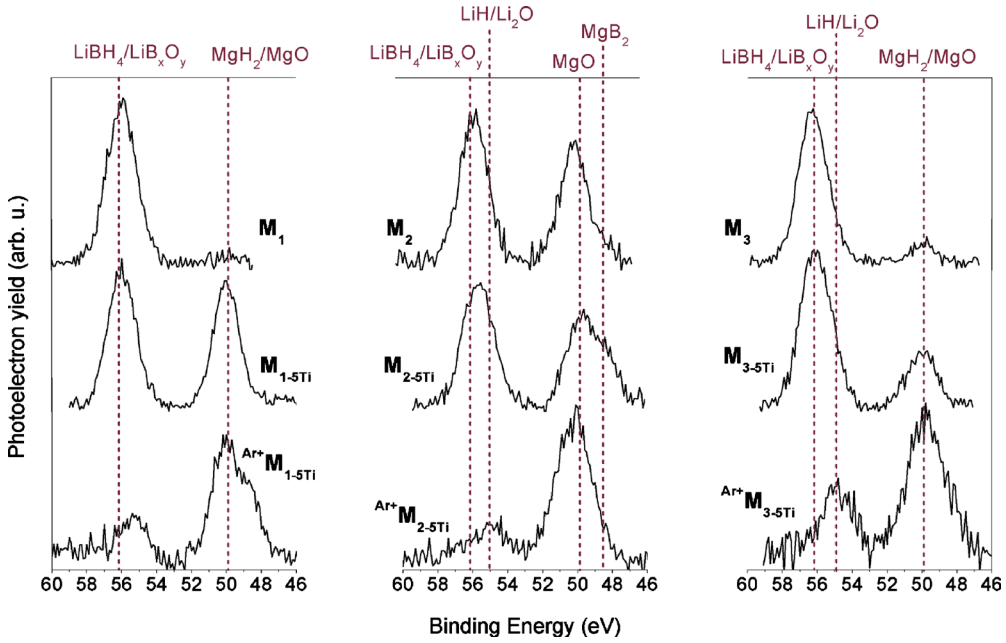

FIG. 3. (Color online) Li 1*s* and Mg 2*p* photoemission peaks for $2LiBH_4+MgH_2$ after ball milling (M_1), desorption (M_2), and one cycle (M_3) and for $2LiBH_4+MgH_2+5$ mol % Ti-iso after ball milling (M_{1-5Ti}), desorption (M_{2-5Ti}) and one cycle (M_{3-5Ti}). Li 1*s* and Mg 2*p* photoemission peaks for $2LiBH_4+MgH_2+5$ mol % Ti-iso for the three sorption stages after one hour Ar^+ sputtering ($^{Ar+}M_{1-5Ti}$, $^{Ar+}M_{2-5Ti}$, and $^{Ar+}M_{3-5Ti}$).

tified at 458.6 and 454.1. The higher binding energy contribution is characteristic of TiO_2 whereas the second one can be attributed to TiB_2 according to the literature.[31] The surface oxidation of the titanium boride reference is clear in Fig. 2.

Figure 3 shows the Li 1*s* and Mg 2*p* photoemission peaks for $2LiBH_4+MgH_2$ and $2LiBH_4+MgH_2+5$ mol % Ti-iso at the three sorption stages (as milled, desorbed and cycled). For samples with additive spectra are also shown for the same stages after one hour Ar^+ sputtering. The labeling of samples is summarized in Table I.

After ball milling, the Li 1*s* peaks look similar in both samples with and without Ti-iso and are centered on the position for the reference $LiBH_4/LiB_xO_y$ at 56.1 eV. A difference between the two samples is, however, clearly marked by the Mg 2*p* peak. In presence of Ti-iso additive, a peak associated to MgH_2/MgO is observed at 49.8 eV whereas only small traces of Mg species were registered in case of the sample without additive. This difference can be explained by the difference observed in TEM measurements performed on the two samples and presented in Fig. 4. Particles with sizes in the range 0.1–1 μm appear in the micrographs with a darker contrast and are identified by EDX as the MgH_2 particles. In addition, a lighter matrix appears surrounding the MgH_2 particles. These areas have been identified as the $LiBH_4$ phase, as determined by EDX by comparison to a pure $LiBH_4$ sample. The Ti-based additive has been detected by EDX in the corresponding sample [Fig. 4(b)]. Detailed analysis of these two samples is given in Ref. 22. However, the distribution of the $LiBH_4$ phase embedding MgH_2 appears to be quite different in presence of the Ti-iso additive. In samples with additive the $LiBH_4$ phase present voids [labeled with arrow in Fig. 4(b)] which can explain the presence of a higher XPS Mg signal as compared to the sample without additive.

After desorption the Li 1*s* peaks shift to lower binding energy in both samples what is compatible with the presence of a contribution associated to $LiBH_4/LiB_xO_y$ and also a contribution corresponding to LiH/Li_2O. This suggests that reaction on surface is not complete most probably due to the presence of surface oxidation species. The reaction is complete in the bulk according to XRD data. For Mg 2*p* peaks a component of MgO, or unreacted MgH_2, is observed at 50 eV. At 48.6 eV a component is identified as MgB_2 in agreement with the peaks in the reference sample. This component appears to be more important in presence of Ti-iso which remarks the effect of the additive. Additionally Mg KLL

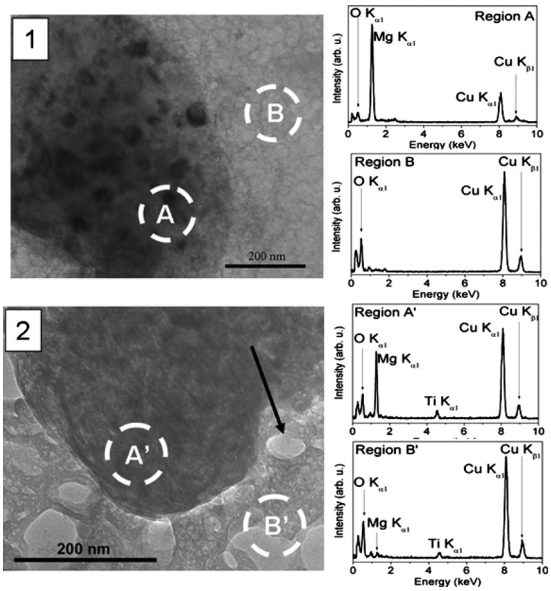

FIG. 4. TEM micrographs and EDX spectra from representative areas (as indicated by the arrows) for the following milled samples: (a) $2LiBH_4+MgH_2$ (M_1) and (b) $2LiBH_4+MgH_2+5$ mol % Ti-iso (M_{1-5Ti}).

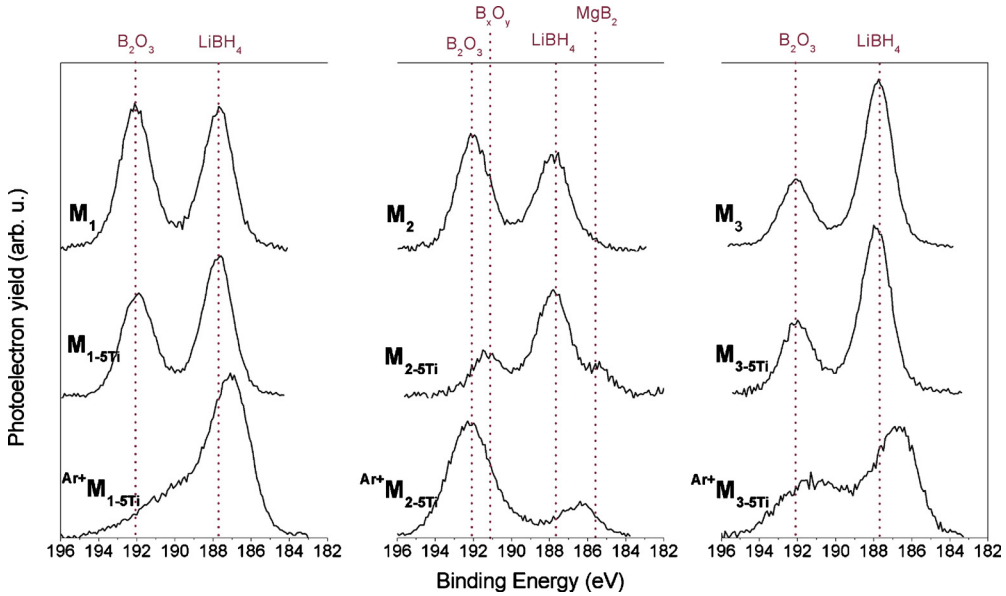

FIG. 5. (Color online) B 1*s* photoemission peaks for $2LiBH_4+MgH_2$ after ball milling (M_1), desorption (M_2), and one cycle (M_3) and for $2LiBH_4+MgH_2+5$ mol % Ti-iso after ball milling (M_{1-5Ti}), desorption (M_{2-5Ti}) and one cycle (M_{3-5Ti}). B 1*s* photoemission peaks for $2LiBH_4+MgH_2+5$ mol % Ti-iso for the three sorption stages after one hour Ar^+ sputtering ($^{Ar+}M_{1-5Ti}$, $^{Ar+}M_{2-5Ti}$, and $^{Ar+}M_{3-5Ti}$).

peaks (not shown) are found to be similar to the one of MgB_2 reference sample. Similarly to Mg 2*p* the Auger peak corresponding to MgB_2 at 1186.3 eV is more intense in presence of Ti-iso additive. The Auger parameter for the MgB_2 component is found equal to 1234.9 similar to the reference sample and close to the values from the literature.[28,30]

As expected for a reversible system, after one cycle the system presents similar chemical states as in the ball milled original state. Two components are clearly identified: the component of $LiBH_4/LiB_xO_y$ at 56.2 eV and the one of MgH_2/MgO at 49.9 eV.

Effects observed after Ar^+ sputtering regarding oxidation state and intensity changes may be analyzed with care due to preferential sputtering effects. A preferential removal of Li and B containing phases seems to indicate the covering of Mg-based phases by the Li-based phases.

Figure 5 shows B 1*s* photoemission peaks for $2LiBH_4+MgH_2$ and $2LiBH_4+MgH_2+5$ mol % Ti-iso at the three sorption stages (as milled, desorbed, and cycled). For samples with additive spectra are also shown for the same stages after one hour Ar^+ sputtering. The labeling of samples is summarized in Table I.

After ball milling, in M_1 and M_{1-5Ti}, the presence of two different chemical states in B 1*s* is clearly observed. The contribution of $LiBH_4$ at 187.8 eV and the one of B_2O_3 oxide at 192.1 eV are in agreement with the literature[31] and our data for the $LiBH_4$ reference material in Fig. 2. After desorption, B 1*s* is quite different for M_2 and M_{2-5Ti}. In M_2 the presence of $LiBH_4$ and boron oxides is clearly identified whereas in M_{2-5Ti} a component at 185.6 eV appears and is attributed to MgB_2 according to B 1*s* binding energy of pure MgB_2. The desorption reaction appears not complete at the surface being favored in the presence of the additive. The presence of oxide species at the surface does not allow detecting a complete transformation to MgB_2. After one cycle the B 1*s* peak shows the two components present in the ball milled samples. A smaller contribution of the oxide is observed which can be explained by the reduction of surface oxidation under the absorption conditions.

After one hour Ar^+ sputtering both milled and one cycled sample show a preferential removal of $LiBH_4$ oxidation products indicating the covering of Mg-based phases by highly dispersed Li-based phases. Nevertheless the effects observed after Ar^+ sputtering regarding oxidation state and intensity changes may be analyzed with care due to preferential sputtering effects.

Figure 6 shows the Ti 2*p* photoemission peaks for $2LiBH_4+MgH_2+5$ mol % Ti-iso at the three sorption stages (as milled, desorbed, and cycled) before and after one hour Ar^+ sputtering. The labeling of samples is summarized in Table I.

For the original milled sample (M_{1-5Ti}), one component at 458.3 eV corresponding to a fully oxidized Ti (IV) is

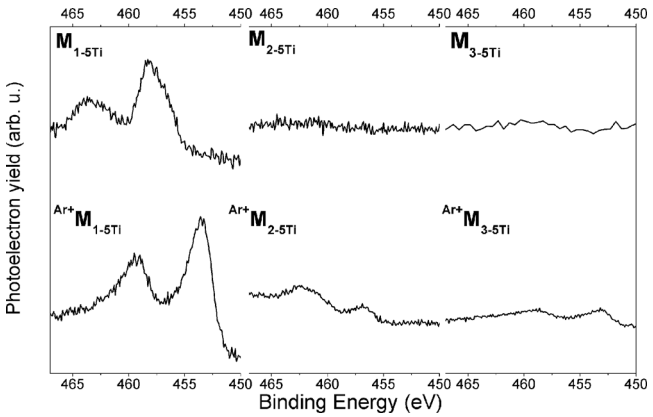

FIG. 6. Ti 2*p* photoemission peaks for $2LiBH_4+MgH_2+5$ mol % Ti-iso after ball milling (M_{1-5Ti}), desorption (M_{2-5Ti}) and one cycle (M_{3-5Ti}) and for the same samples after one hour Ar^+ sputtering ($^{Ar+}M_{1-5Ti}$, $^{Ar+}M_{2-5Ti}$, and $^{Ar+}M_{3-5Ti}$)

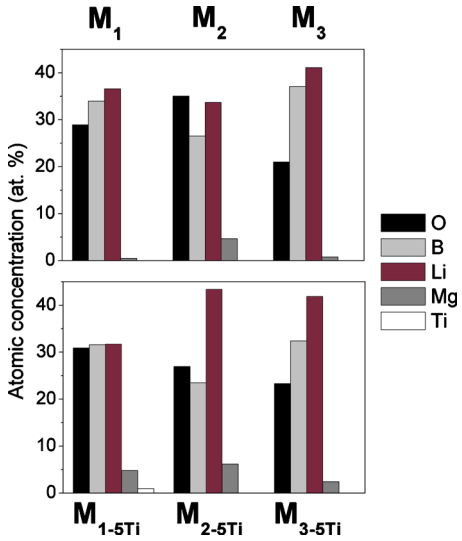

FIG. 7. (Color online) Atomic composition for $2LiBH_4+MgH_2$ after ball milling (M_1), desorption (M_2) and one cycle (M_3) and for $2LiBH_4+MgH_2$ +5 mol % Ti-iso after ball milling (M_{1-5Ti}), desorption (M_{2-5Ti}) and one cycle (M_{3-5Ti}).

clearly identified. Shoulders at lower binding energies are attributed to reduced oxides, like Ti_2O_3,[33] which could be formed during the milling process and are also present at the surface. These oxide like species are likely the main products of the titanium isopropoxide decomposition. Figure 6 shows that Ti species are not further detected on the surface upon desorption and cycling (samples M_{2-5Ti} and M_{3-5Ti}), indicating a migration of Ti species into the bulk. Therefore, the formation of titanium boride species cannot be observed by XPS. These active species have been unequivocally detected by previous XAS and TEM studies.[19–21]

Figure 6 also shows the Ti $2p$ photoelectron peaks for the same samples after one hour Ar^+ sputtering treatment. The removal of material, by long time sputtering, shows the presence of the Ti phases in the cycled samples in the subsurface region. In sample $^{Ar+}M_{1-5Ti}$, Ar^+ sputtering produces reduction in titanium oxide, which likely is due to preferential sputtering of oxygen.[33] This effect does not allow getting conclusions on the oxidation state of Ti in the bulk of cycled samples. Nevertheless, the migration of Ti species from the surface to the bulk during the first desorption is the main conclusion observed from the Ti $2p$ peak analysis.

A quantitative analysis of O $1s$, B $1s$, Li $1s$, Mg $2p$, and Ti $2p$ photoelectron peaks has been carried out and the corresponding atomic concentrations have been calculated. In Fig. 7 is represented the surface atomic composition for $2LiBH_4+MgH_2$ and $2LiBH_4+MgH_2+5$ mol % Ti-iso after ball milling (M_1 and M_{1-5Ti}), desorption (M_2 and M_{2-5Ti}) and one cycle (M_3 and M_{3-5Ti}).

After ball milling the Li/B ratio is found to be close to 1 for both samples, with and without additive (M_1 and M_{1-5Ti}), corresponding to the ratio in $LiBH_4$. The difference observed previously on Mg $2p$ intensity between M_1 and M_{1-5Ti} is confirmed by the Mg atomic concentration. The oxygen concentration of about 30% can be explained by the high sensitivity and the reactivity to water and oxygen of hydrides as well as from the oxygen brought by the additive. The concentration of Ti is observed for M_{1-5Ti} and found to be very small due to low Ti concentration in the samples and its distribution on the surface and in the bulk.

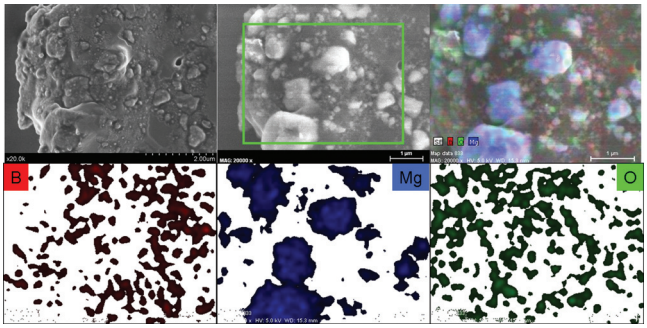

FIG. 8. (Color) SEM micrographs of $2LiBH_4+MgH_2$ after ball milling. Up-left: image at 2 kV. Up-middle: image at 5 kV. Up-right: elemental mapping of B (red), Mg (blue), O (green), and secondary electrons (white). Individual distributions of each element in the sample are presented in the bottom.

After desorption the reaction is not complete on the surface as already observed in the study of the photoelectrons peaks. In fact there is an excess of the B signal as compared to Mg what indicates that boron is forming not only MgB_2, but also $LiBH_4$ and oxidized species like LiB_xO_y or boron oxides. The Mg concentration is found here higher than in ball milled samples. In Ref. 22 a detailed TEM study has shown that elongated crystals of MgB_2 are dispersed in a LiH matrix whereas in the milled state MgH_2 are agglomerated into particles surrounded by $LiBH_4$. The higher atomic concentration of Mg for the M_{2-5Ti} sample indicates again the favorable effect of Ti-based additives to improve the heterogeneous nucleation of MgB_2 (higher dispersion of this phase). The O atomic concentration is found lower in the presence of additive which can maybe due to the migration of the O containing species associated to Ti-iso into the bulk as it has been shown in Fig. 6.

After one cycle, the same observation on Mg and Li concentration can be done as for ball milled sample. Li and B signals appear correlated showing high intensity as corresponds to the high dispersion of $LiBH_4$ onto the MgH_2 bigger crystals. Single crystals of MgH_2 of respectively 1100 and 760 nm for M_3 and M_{3-5Ti} have been observed by TEM.[22] In presence of Ti-iso, the MgH_2 crystals are smaller and have, therefore, a higher surface area which is in good agreement with the higher Mg concentration at the surface found here. A significant decrease of oxygen concentration is also observed after one cycle which may be due to the heating at 350 °C under 50 bar H_2.

C. Scanning electron microscopy (SEM)

Morphology and elemental composition studies in the samples have been undertaken combining SEM with elemental mapping by EDX. Distributions of B, O, Mg and Ti were, therefore, measured as Li is out of the detection capacity of the EDX detector. The comparison between samples without and with additive was done for 10 mol% additive to improve the signal in the Ti distribution maps.

In Fig. 8 SEM shows the morphology of $2LiBH_4$

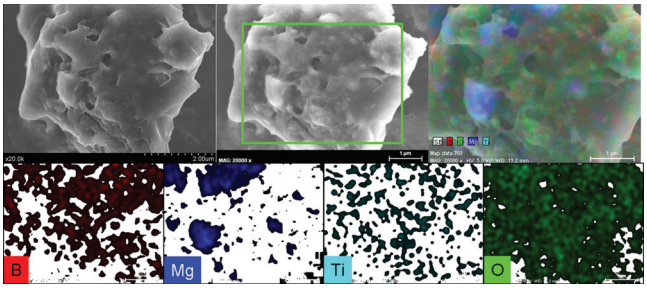

FIG. 9. (Color) SEM micrographs of $2LiBH_4+MgH_2+10$ mol % Ti-iso after ball milling. Up-left: image at 2 kV. Up-middle: image at 5 kV. Up-right: elemental mapping of B (red), Mg (blue), Ti (turquoise), O (green), and secondary electrons at 5 kV. Individual distributions of each element in the sample are presented in the bottom.

$+MgH_2$ after ball milling as well as B, O and Mg distribution for the delimited zone. The secondary electron micrograph at 5 kV (up-middle) shows a darker matrix composed mainly of B and O and particles of lighter contrast which are mainly composed of Mg and few O. Therefore, MgH_2 particles appear to be surrounded by a matrix of $LiBH_4$ and both of them are superficially oxidized. In addition to SEM observation, micrograph obtained in TE (transmitted electron) mode (not shown) appears similar to TEM micrograph presented in Fig. 4 in this paper. Sizes of MgH_2 grains appear to range from hundreds of nm to around 1 micron.

Figure 9 shows SEM micrographs of $2LiBH_4+MgH_2+10$ mol% Ti-iso as well as an elemental mapping for the area delimited by the green square. Similarly to the sample without additive most of the MgH_2 particles appear surrounded with $LiBH_4$ and both of them are also strongly oxidized which is in agreement with TEM observations.[22] Oxygen appears to be in higher concentration as compared to the sample without additive; this can be due to oxygen contained in the additive. The most important feature here is the localization of Ti that appears uniformly distributed in the sample whereas zones with high Mg concentration are clearly distinguished.

It should be mentioned here that sample decomposition was observed under electron beam irradiation with the $LiBH_4$ phase being the more sensible one as already observed during TEM examinations.[22]

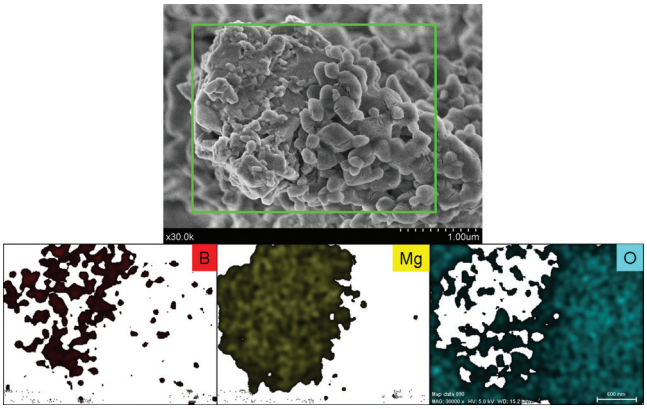

FIG. 10. (Color) SEM micrographs of $2LiBH_4+MgH_2$ after desorption. Up-left: image at 2 kV. Bottom: elemental individual distribution of B (red), Mg (yellow) and O (turquoise) in the selected green area.

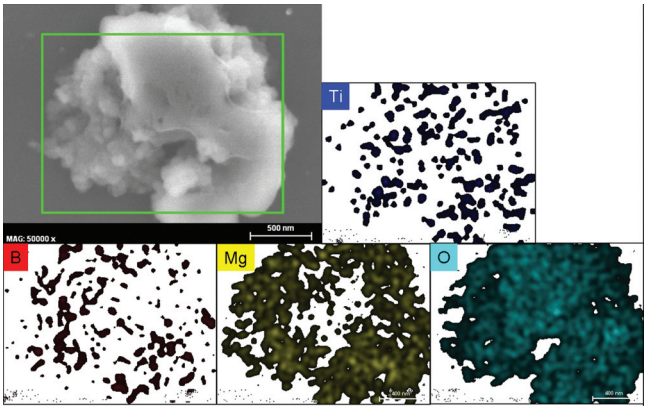

FIG. 11. (Color) SEM micrograph of $2LiBH_4+MgH_2+10$ mol % Ti-iso after desorption. Up-left: image at 5 kV. Up-right: elemental individual distribution of Ti (blue) in the selected green area. Bottom: elemental individual distribution of B (red), Mg (yellow) and O (turquoise) in the selected green area.

Figure 10 shows a secondary electron micrograph for $2LiBH_4+MgH_2$ after desorption. B, O, and Mg distributions were also obtained for the delimited zone. Elemental mapping shows that there are regions mainly composed of Mg and B which correspond to the MgB_2 phase. Oxygen in this area is mainly found in the regions outside the MgB_2 and it can likely be the result of the partial decomposition coupled to oxidation of the LiH phase. This phase has been shown to be unstable under the beam even at 5 kV as well as under electron beam in TEM experiments.

In Fig. 11 results are presented for $2LiBH_4+MgH_2+10$ mol % Ti-iso after desorption. Regions rich in Mg and with a high concentration of B are differentiated confirming the presence of MgB_2 and LiH phases. Oxygen is detected in all regions of the sample. The identification of separated MgB_2 and LiH phases is more difficult in these samples because we are in the limit of lateral resolution of our EDX analysis. The most important feature here is the localization of Ti that appears uniformly dispersed in the sample.

Results for sample $2LiBH_4+MgH_2$ after one full dehydrogenation-rehydrogenation cycle are presented in Fig. 12. In the secondary electron image large particles can be clearly distinguished with a dark contrast. These particles show in the elemental mapping to be mainly composed of Mg. This confirms the micrometer particle size of MgH_2 af-

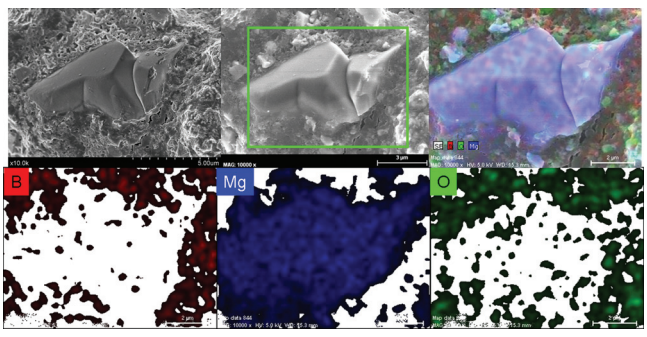

FIG. 12. (Color) SEM micrographs of $2LiBH_4+MgH_2$ after one cycle. Up-left: image at 2 kV. Up-middle: image at 5 kV. Up-right: elemental mapping of B (red), Mg (blue), O (green), and secondary electrons (white). Individual distributions of each element in the sample are presented in the bottom.

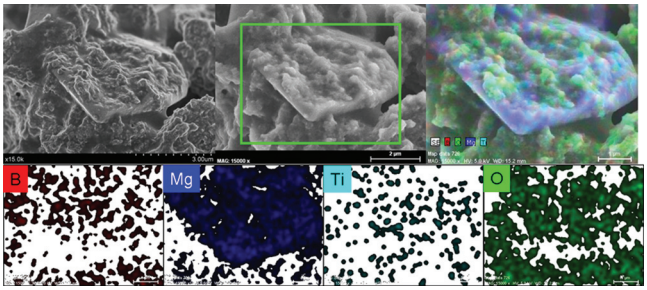

FIG. 13. (Color) SEM micrographs of $2LiBH_4+MgH_2+10$ mol % Ti-iso after one cycle. Up-left: image at 2 kV. Up-middle: image at 5 kV. Up-right: elemental mapping of B (red), Mg (blue), Ti (turquoise), O (green), and secondary electrons (white). Individual distributions of each element in the sample are presented in the bottom.

ter cycling as previously observed by TEM.[22] The MgH_2 particle appears to be surrounded by a matrix of material which elemental mapping shows a high concentration of B and O as expected for the $LiBH_4$ phase. The re-charging reaction appears, therefore, fully reversible as required for hydrogen storage applications. The texture of the $LiBH_4$ matrix shows a strong rugosity most probably due to the characteristic decomposition of borohydrides under electron beam irradiation.[22,34,35] Oxygen appears in most regions although some MgH_2 particles are poorer in oxygen (as the one showed in Fig. 12). This can be probably due to the highest reactivity of $LiBH_4$ to oxygen as compared to MgH_2.

Results for sample $2LiBH_4+MgH_2+10$ mol % Ti-iso after one cycle are presented in Fig. 13. Also in this case micrometer range particles of MgH_2 are clearly identified in the micrograph as confirmed by the high concentration of Mg marked in blue. MgH_2 particles are covered with materials rich in B which corresponds to $LiBH_4$. Compared to the sample without additive the MgH_2 particles in $2LiBH_4+MgH_2+10$ mol % Ti-iso appears to be more oxidized what can be explained by the oxygen contribution of the additive itself. Titanium appears uniformly dispersed in the sample.

IV. DISCUSSION

XRD and volumetric data[15] show that H_2 sorption reactions in the $LiBH_4-MgH_2$ RHC system are nearly complete in the bulk and fully reversible in the conditions employed in the present paper (400 °C and 5 bar for desorption and 350 °C and 50 bar for absorption). In previous works[20–22] it has been also demonstrated that the Ti based additive is present after ball milling as Ti oxide like species whereas upon cycling the additive migrates to the bulk as a mix of TiB_2 and Ti_2O_3 species. It has been pointed out that the Ti-boride active phase may play its main role at the $LiBH_4-Mg$ interface in the bulk where it is promoting the heterogeneous nucleation of the MgB_2. The rate limiting process, related to the observed plateau in dehydrogenation measurements, appears to be, not the hydrogen diffusion from the surface, but the nucleation of the MgB_2 phase to be formed.

The XPS data in this paper also demonstrate the reversibility of the system upon cycling. Although the desorption reaction is not complete at the surface, the presence of the additive is clearly favoring the formation of MgB_2, and therefore, the reaction kinetics in agreement with previously proposed mechanisms.[20–22] The presence of oxide species at the surface does not allow detecting a complete transformation to MgB_2 by XPS. The additive by enhancing the heterogeneous nucleation of MgB_2 favors its dispersion what explain the increase in the XPS signal for this species and the faster rehydrogenation kinetics.

The location and determination of chemical state of the Ti-additive is a major question to understand the role of additives in these systems. From the XPS data shown in this work, it has been concluded that after ball milling oxidized Ti(IV) species are present at the surface. The formation of active TiB_2 species after first desorption could not be observed as this phase migrates to the bulk. This is, however, a very important result that confirms the role of the additive at the interfaces in bulk material. No conclusions can be drawn from sputtering experiments about chemical state of Ti due to preferential sputtering effects. At that point the information obtained by SEM/EDX elemental maps is very important and complementary to surface analysis. The Ti phases appear in all the samples for the three sorption steps well dispersed and uniformly distributed in the material. This is a main result from this paper showing that the use of the Ti isopropoxide precursor as additive, together with the ball milling processing, are very favorable conditions to produce the high dispersion of the additive.

The interpretation of the quantitative XPS analysis indicates that the Li-based phases are highly dispersed at the surface while the Mg-based ones appear, either partially covered by the Li-based phases, or forming bigger grains. This is particularly clear in the SEM/EDX images for the case of milled and cycled samples. The MgH_2 phase shows particles of hundreds of nanometer to 1 μm size while the $LiBH_4$ is well dispersed surrounding the magnesium hydride.

Both SEM/EDX and XPS analysis show some grain refinement in the presence of the additive. Specifically in samples with additive the dispersion of the MgB_2 phase and the reduction in particles size for MgH_2 after cycling are clearly observed in our measurements. These effects, together with the enhancement of the heterogeneous nucleation of MgB_2, are the main factors improving the kinetic of the sorption reactions.

V. CONCLUSIONS

An exhaustive surface characterization by XPS is reported here for the $LiBH_4-MgH_2$ RHC system with and without the Ti-iso additive. SEM/EDX analysis coupled to elemental maps are presented for the first time for this system for all three stages: as milled, dehydrogenated and rehydrogenated. Complementarities between XPS and SEM/EDX have been shown to be very useful to study both distribution and chemical state of the elements particularly for the Ti-based phases.

The study of the Li 1*s*, Mg 2*p*, and B 1*s* photoelectron peaks show that sorption reactions are not complete at the surface more likely due to the presence of oxidized species. Nevertheless the XPS data show that the presence of the

additive is clearly favoring the formation and dispersion of MgB_2 in agreement with the previous proposed mechanism.[18–22]

The combined use of XPS and SEM/EDX elemental mapping shows that the Ti-based additive is well dispersed and uniformly distributed in the material migrating to the bulk during the first desorption processes. The formation of active TiB_2 species could not be detected by XPS as this phase migrates from the surface to the bulk. The high dispersion of the Ti species (Ti-oxide and Ti-boride) at the bulk phase boundaries is favoring the heterogeneous nucleation of MgB_2 and thereby leading to smaller grains of the formed phases, increasing interfacial area and improving the kinetics in both charging and de-charging processes.

The quantitative XPS and SEM/EDX analyses show that the $LiBH_4$ phase is highly dispersed and partially covering bigger MgH_2 particles. These latter particles appear to have sizes from hundreds of nm to 1 μm in good agreement with TEM results detailed in Deprez *et al.*[22]

All samples are found to be superficially oxidized. A moderate decrease in the oxygen content is, however, observed by XPS after one cycle what could be explained by the absorption conditions. The Ti-isopropoxide additive is also an additional source of oxygen in these samples.

In summary, the combined use of a surface characterization technique, like XPS, with the microstructural analysis undertaken in the SEM microscope, gave new data regarding microstructural characterization, grain size, surface composition, and elemental distribution in the microscale for the $LiBH_4+MgH_2$ RHC system with Ti-iso additive.

ACKNOWLEDGMENTS

Financial support by the Marie Curie Program (Grant No. MRTN-CT-2006-035366), as well as the Spanish MICINN (Grant No. CTQ2009-13440), and the Junta de Andalucía are acknowledged.

[1]L. Schlapbach and A. Züttel, Nature (London) **414**, 353 (2001).
[2]2005 FY Annual Progress Report for the DOE Hydrogen Program, US Government Printing Office, Washington, DC, November 2005, www.hydrogen.energy.gov/annual_progress05.html
[3]J. Huot, G. Liang, S. Boily, A. Van Neste, and R. Schulz, J. Alloys Compd. **293–295**, 495 (1999).
[4]O. Friedrichs, J. C. Sánchez-López, C. López-Cartes, T. Klassen, R. Bormann, and A. Fernández, J. Phys. Chem. B **110**, 7845 (2006).
[5]W. Oelerich, T. Klassen, and R. Bormann, Adv. Eng. Mater. **3**, 487 (2001).
[6]G. Barkhordarian, T. Klassen, and R. Bormann, Scr. Mater. **49**, 213 (2003).
[7]A. Züttel, S. Rentsch, P. Fischer, P. Wenger, P. Sudan, Ph. Mauron, and Ch. Emmenegger, J. Alloys Compd. **356–357**, 515 (2003).
[8]B. Bogdanovic and M. Schwickardi, J. Alloys Compd. **253–254**, 1 (1997).
[9]N. L. Rosi, J. Eckert, M. Eddaoudi, D. T. Vodak, M. O'Keefe, and O. M. Yaghi, Science **300**, 1127 (2003).
[10]A. Züttel, P. Wenger, S. Rentsch, P. Sudan, Ph. Mauron, and Ch. Emmenegger, J. Power Sources **118**, 1 (2003).
[11]S. Orimo, Y. Nakamori, and A. Züttel, Mater. Sci. Eng., B **108**, 51 (2004).
[12]O. Friedrichs, A. Borgschulte, S. Kato, F. Buchter, R. Gremaud, A. Remhof, and A. Züttel, Chem.-Eur. J. **15**, 5531 (2009).
[13]J. J. Vajo, S. L. Skeith, and F. Mertens, Chem. Phys. Lett. **109**, 3719 (2005).
[14]G. Barkhordarian, T. Klassen, M. Dornheim, and R. Bormann, J. Alloys Compd. **440**, L18 (2007).
[15]U. Bösenberg, S. Doppiu, L. Mosegaard, G. Barkhordarian, N. Eigen, A. Borgschulte, T. R. Jensen, Y. Cerenius, O. Gutfleisch, T. Klassen, M. Dornheim, and R. Bormann, Acta Mater. **55**, 3951 (2007).
[16]J. J. Vajo, T. T. Salguero, A. F. Gross, S. L. Skeith, and G. L. Olson, J. Alloys Compd. **446–447**, 409 (2007).
[17]M. Dornheim, S. Doppiu, G. Barkhordarian, U. Boesenberg, T. Klassen, O. Gutfleisch, and R. Bormann, Viewpoint Set in Scripta Materialia **56**, 841 (2007).
[18]U. Bösenberg, U. Vainio, P. K. Pranzas, J. M. Bellosta von Colbe, G. Goerigk, E. Welter, M. Dornheim, A. Schreyer, and R. Bormann, Nanotechnology **20**, 204003 (2009).
[19]U. Bösenberg, J. W. Kim, D. Gosslar, N. Eigen, T. R. Jensen, J. M. Bellosta von Colbe, Y. Zhou, M. Dahms, D. H. Kim, R. Günther, Y. W. Cho, K. H. Oh, T. Klassen, R. Bormann, and M. Dornheim, Acta Mater. **58**, 3381 (2010).
[20]E. Deprez, M. A. Muñoz-Márquez, M. A. Roldán, C. Prestipino, F. J. Palomares, C. Bonatto Minella, U. Bösenberg, M. Dornheim, R. Bormann, and A. Fernández, J. Phys. Chem. C **114**, 3309 (2010).
[21]A. Fernández, E. Deprez, and O. Friedrichs (submitted).
[22]E. Deprez, A. Justo, T. C. Rojas, C. López-Cartés, C. Bonatto Minella, U. Bösenberg, M. Dornheim, R. Bormann, and A. Fernández, Acta Mater. **58**, 5683 (2010).
[23]O. Friedrichs, J. C. Sánchez-López, C. López-cartes, M. Dornheim, T. Klassen, R. Bormann, and A. Fernández, Appl. Surf. Sci. **252**, 2334 (2006).
[24]B. R. Strohmeier, Surf. Interface Anal. **15**, 51 (1990).
[25]Y. Kojima, K. Tange, S. Hino, S. Isobe, M. Tsubota, K. Nakamura, M. Nakatake, H. Miyaoka, H. Yamamoto, and T. Ichikawa, J. Mater. Res. **24**, 2185 (2009).
[26]J. P. Contour, A. Salesse, M. Froment, M. Garreau, J. Thevenin, and D. Warin, J. Microsc. Spectrosc. Electron. **4**, 483 (1979).
[27]Y. Baer, P. H. Citrin, and G. K. Wertheim, Phys. Rev. Lett. **37**, 49 (1976).
[28]R. P. Vasquez, C. U. Jung, M.-S. park, H.-J. Kim, J.Y. Kim, and S.-I. Lee, Phys. Rev. B **64**, 052510 (2001).
[29]S. Ardizzone, C. L. Bianchi, M. Fadoni, and B. Vercelli, Appl. Surf. Sci. **119**, 253 (1997).
[30]A. Serquis, Y. T. Zhu, D. E. Peterson, F. M. Mueller, R. K. Schulze, V. F. Nesterenko, and S. S. Indrakanti, Appl. Phys. Lett. **80**, 4401 (2002).
[31]Y. H. Guo, X. B. Yu, L. Gao, G. L. Xia, Z. P. Guo, and H. K. Liu, Energy Environ. Sci. **3**, 465 (2010).
[32]W. E. Moddeman, A. R. Burke, W. C. Bowling, and D. S. Foose, Surf. Interface Anal. **14**, 224 (1989).
[33]L. Soriano, M. Abbate, J. Vogel, J. F. Fuggle, A. Fernández, A. R. González-Elipe, M. Sacchi, and J. M. Sanz, Surf. Sci. **290**, 427 (1993).
[34]M. Fichtner, Z. Zhao-Karger, J. Hu, A. Roth, and P. Weidler, Nanotechnology **20**, 204029 (2009).
[35]B. Bogdanovic, M. Felderhoff, and G. Streukens, J. Serb. Chem. Soc. **74**, 183 (2009).